Shear-wave propagation in orthorhombic Phenolic CE: A comparison of numerical and physical modelling

Georg Rümpker* and R. James Brown

ABSTRACT

In this paper we analyze effects of shear-wave propagation in orthorhombic Phenolic CE (PCE). This industrial laminate provides a physical model for the study of wave propagation in anisotropic media and has been used in a number of laboratory experiments. In a recent experiment by Brown et al. (1993) polarity reversals were found on seismogram traces along two profiles through a sphere of PCE. The observations were attributed to the rapid variation of polarization in the neighbourhood of slowness surface conical points (point singularities). Based on numerical modelling experiments we attempt an interpretation of these observations. The numerical results show amplitude variations similar to those observed in the physical modelling. The amplitude variations for receiver positions along a symmetry plane of the anisotropic medium may indeed be attributed to rapid polarization changes due to conical points. However, the numerical examples indicate that relatively smooth variations of the displacement on crossing a symmetry plane can result in rapid amplitude variations (polarity reversals) on seismogram traces, depending on the transmitter/receiver configuration used. The calculated seismograms also show characteristic (Hilbert-transform type) waveforms due to wavefront folding. This folding is a direct results of slowness surface conical points and the related waveform characteristics may be used in future experiments to detect conical point effects. However, the detectability of these waveform variations depends strongly on the frequency range emitted by the source.

INTRODUCTION

In recent years considerable effort has been made to physically model elastic wave propagation effects in anisotropic media. Cheadle et al. (1991) first employed Phenolic CE (PCE) to model an anisotropic elastic medium. It was found that the variations of the quasi-longitudinal (P) and the two quasi-shear (S and T) wave speeds with direction resembled those of an orthorhombic elastic medium. The corresponding elastic stiffnesses were determined form observed body-wave velocities. In another experiment by Brown et al. (1991) a slab of PCE was used to model the effects of multiple receiver offsets on anisotropic wave propagation. Pronounced shear-wave splitting was observed in seismogram records from off-symmetry planes.

In a more recent study by Brown et al. (1993) the PCE model was used to analyze the effects of slowness surface conical points (or point singularities, see e.g. Crampin, 1981) on the propagation of shear waves through a homogeneous sphere of PCE laminate. Piezoelectric source and receiver transducers, placed in antipodal positions on a sphere, were used to record seismogram sections along two orthogonal profiles. Using experimentally determined stiffness values for the sphere, sections through the phase and group velocity surfaces corresponding to the recorded

* Department of Geological Sciences, Queen's University, Kingston, Ontario K7L 3N6

seismogram sections were calculated. The numerical results showed the existence of a conical point on the slowness surface (or similarly on the phase-velocity surface) in the 31-symmetry plane. The profiles were recorded along a line corresponding to this symmetry plane and along a line perpendicular to it (Figure 1). The most striking feature of the seismograms observed was a polarity reversal for arrivals on the cross-component records (combinations of radial and transverse transmitter/receiver configurations) for the two profiles through the sphere (Figures 2 and 3). The polarity reversals were attributed to rapid variations of the polarization in the neighbourhood of conical points on the slowness surface.

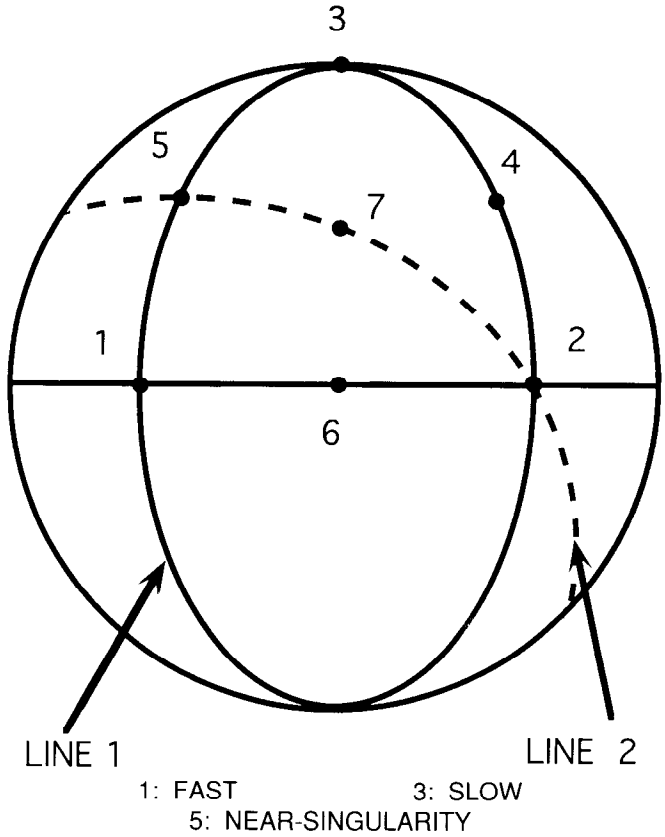

FIG. 1. The two perpendicular lines, Line 1 (solid) and Line 2 (dashed). The symmetry axes (1, 2 and 3) are labelled as well as the directions (4, 5 and 6) halfway between axes. Point 7 marks the direction equidistant from the three axes.

In the study presented here we will investigate the relationship between slowness surface conical points and related seismogram features more closely by means of numerically calculated shear-wave seismograms. A direct comparison between numerically calculated and observed seismograms for these physical models of anisotropic media has not been carried out before and we expect that the numerical results will guide the interpretation of the complex features observed. First, we try to illuminate the wave propagation effects of conical points in a homogeneous orthorhombic material. Therefore, we show examples of shear wavefronts and high-frequency seismograms for receiver directions at and close to the acoustic axis (i.e. the axis in slowness space that points from the origin into the direction (p_x, p_y, p_z) of a conical point or point singularity on the slowness surface). In a second step we will numerically model and analyze some of the effects observed in the experiment by Brown et al. (1993) for an orthorhombic sphere of PCE. For simplicity, we assume wave propagation through a homogeneous orthorhombic material. The transmitter is

modelled as a point source and effects due to reflection and refraction of phases on the sphere boundary will not be included. Nevertheless, we hope that some of the basic observations can be explained with this simple model and that the results my guide the setup and observations of future experiments.

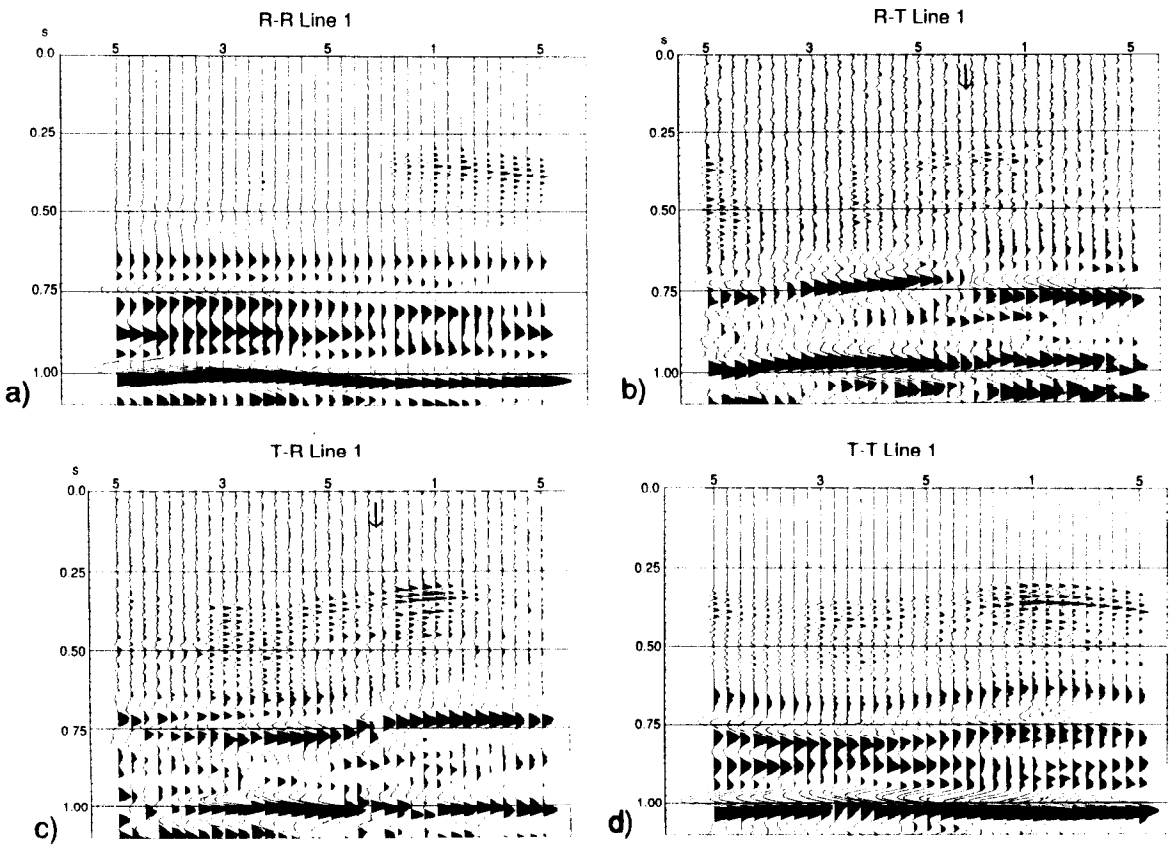

FIG. 2. Four-component seismograms for Line 1. The R-T and T-R seismograms have an applied gain factor of 2. Traveltimes have been scaled up by a factor of 10^4. Arrows on (b) and (c) indicate the approximate position of the polarity change.

EFFECTS OF CONICAL POINTS IN ORTHORHOMBIC PCE

The equation for the slowness surface for a general anisotropic medium may be given in the form (e.g., Fedorov, 1968; Musgrave, 1970; Helbig, 1994):

$$\det\left|c_{ijkl}p_i p_l - \rho\delta_{jk}\right| = 0 \qquad (1)$$

where c_{ijkl} is the tensor of elastic stiffnesses, p_i the slowness and ρ the density. For an orthorhombic medium there are nine independent elastic stiffnesses of nonzero value and the usual symmetry conditions for the tensor c_{ijkl} apply. For given horizontal

slowness components p_x and p_y, equation (1) may be regarded as a sixth-order equation for the vertical slowness p_z corresponding to three "upgoing" and three "downgoing" waves. On the other hand, for each wavefront normal, $n_i = vp_i$, we may find three eigenvalues v corresponding to the phase velocities of one quasi-longitudinal (P) and two quasi-shear (S and T) waves. Here, we use values for the elastic stiffnesses c_{ijkl} and the density ρ determined by Brown et al. (1993) for a sphere of PCE laminate. This will allow a direct comparison with the results of the physical modelling.

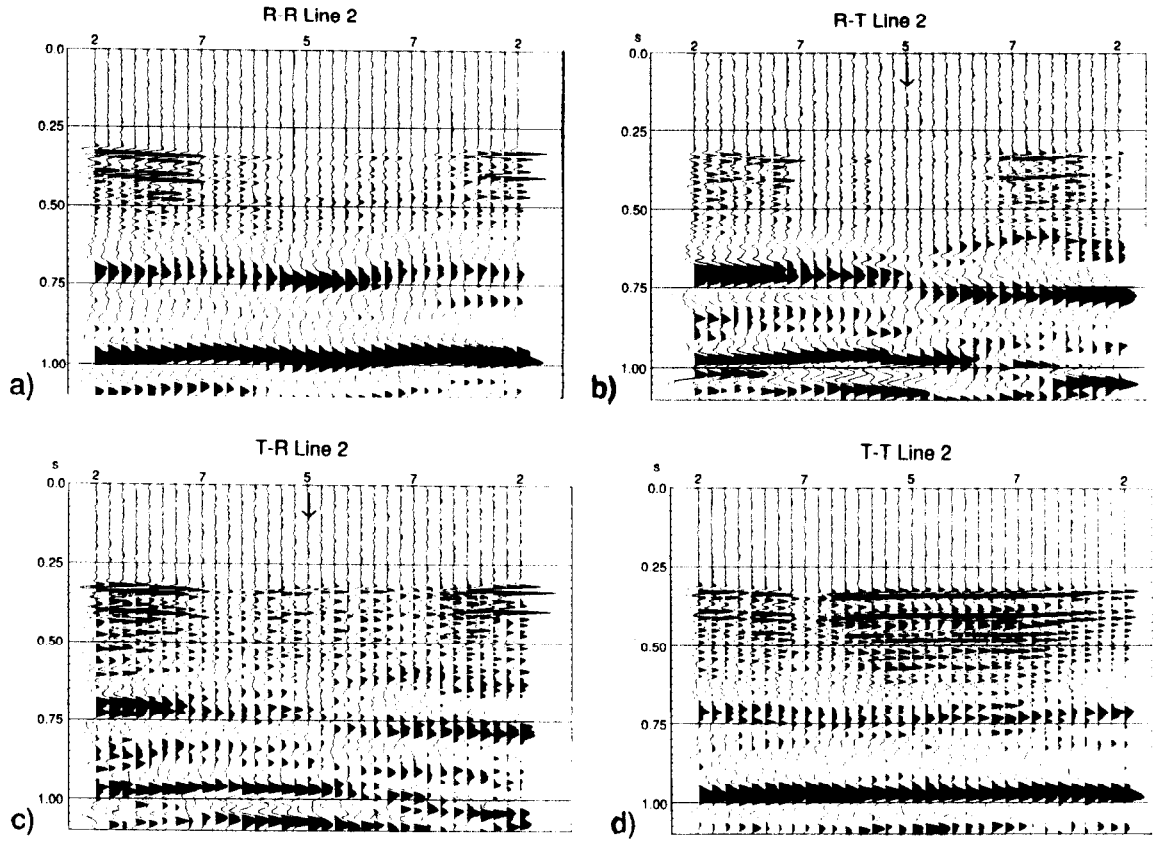

FIG. 3. Four-component seismograms for Line 2. The seismograms have the same applied gain factor. Otherwise as for Figure 2.

Figure 4 shows three sections of the shear-wave slowness along symmetry planes of the slowness surface and corresponding sections of the wave (group) velocity calculated for these values of the elastic stiffnesses. The 1-axis and the 3-axis coincide with the fastest and slowest directions of the P wave velocity, respectively. Results are only shown for the two shear waves. There are two conical points in the 2-3 plane and one more in the 3-1 plane of the slowness surface. As a result of conical points on the slowness surface the sections of the S-wave velocity exhibit small gaps, whereas the curve for the T wave velocity intersects itself and is multivalued. This is due to the fact that slowness and wave surface are related by a polar reciprocal relationship: The direction of the group velocity vector is given by the normal to the slowness surface.

Note that the sections of the group velocity shown in Figure 4 are not "complete": only group velocities are shown that relate to slowness values in symmetry planes of the slowness surface. The complete group velocity sections should also include values corresponding to slownesses out of the symmetry plane but with "in-plane" slowness-surface normals. The two conical points in the 2-3 plane are not stable with respect to small changes in the material properties (see Brown et al., 1993). Therefore, we will concentrate on the effects of the conical point in the 3-1 plane. By making use of analytical expressions for the slowness surface sections in symmetry planes (see e.g. Musgrave (1970, 1981)), the position of the angular distance from the 3-axis can be calculated. We find this distance to be 63.1°.

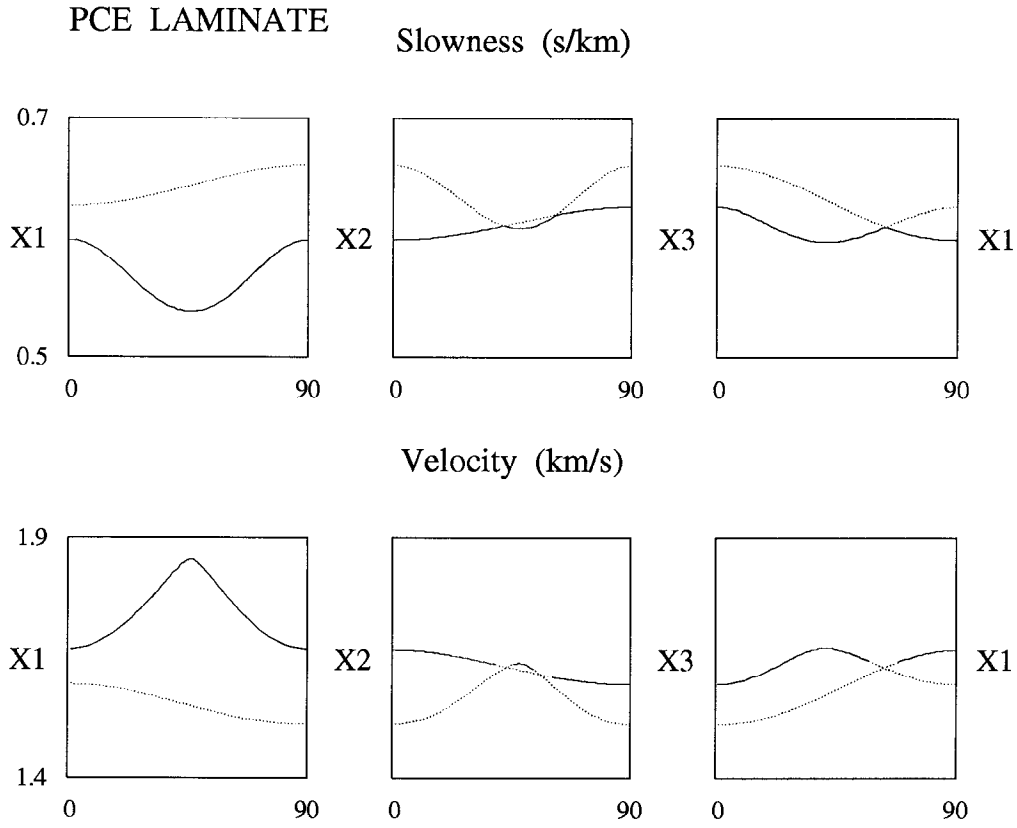

FIG. 4. Shear-wave slowness and group velocity in symmetry planes of the PCE laminate sphere. The stiffnesses and density used are reported by Brown et al. (1993). The thick and dotted lines refer to the fast (S), and slow (T) shear waves, respectively.

To further investigate the effect of out-of-plane slowness contributions we show contours of the vertical slowness p_z as a function of the horizontal slownesses p_x and p_y for the S and T sheets of the slowness surface in the neighbourhood of the conical point (Figure 5). The coordinate system has been rotated with the p_z-axis in the direction of the acoustic axis. The 3-1 plane coincides now with the plane $p_x = 0$ and the p_y-axis is in the 3-1 plane. The maximum on the S-wave slowness sheet and the minimum on the T-wave sheet mark the position of the conical point, where the two sheets touch like two cones placed tip to tip. There are two maxima on the T-wave sheet in the 3-1 symmetry plane and two saddle points slightly out of this plane. The x and y-components of the slowness-surface normals at these "stationary points" on the T-wave sheet vanish and give rise to four overlapping geometrical arrivals in the T-wave seismogram for a receiver on the acoustic axis ($x = y = 0$). [See Buchwald (1959) for a

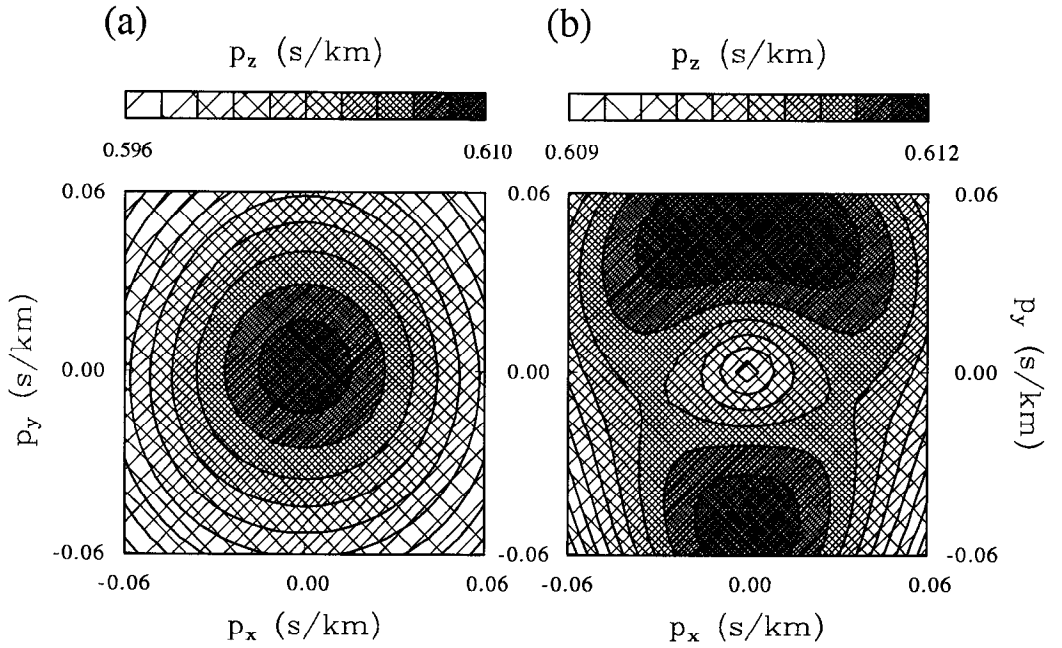

FIG. 5. The vertical slowness p_z as a function of the horizontal slownesses p_x, p_y in the neighbourhood of the conical point at the origin for (**a**) the S wave and (**b**) the T wave.

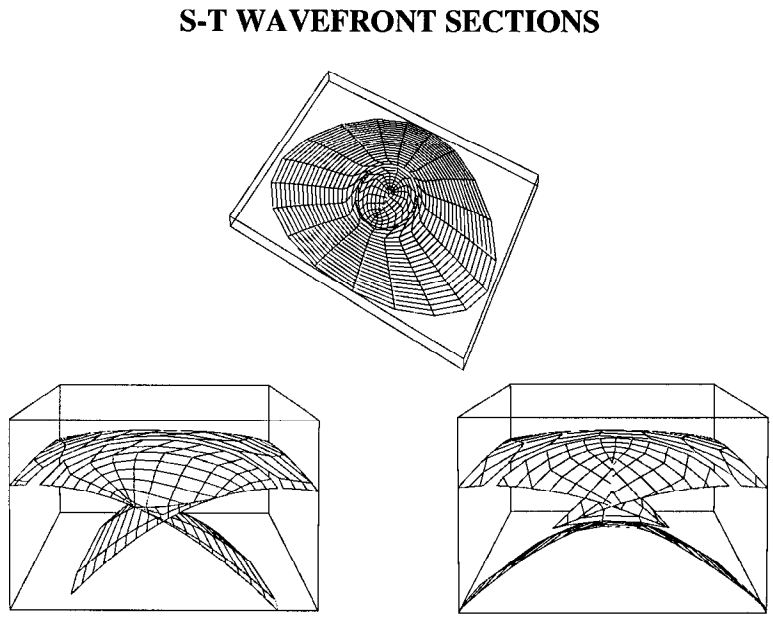

FIG. 6. Sections of the two shear wavefronts calculated from slowness values around the acoustic axis: (**a**) viewed obliquely above the z axis; note the hole in the (light) S wavefront filled by the (dark) T wavefront; (**b**) and (**c**) show sections for $x \leq 0$ and (c) $y \geq 0.$, respectively. A small gap between the S and the folded T wavefronts is left for purposes of representation.

more complete explanation of this]. At the conical point, the normal to the slowness surface is not defined. In fact, the normal varies discontinuously for all curves on the slowness surface that pass through the conical point. This gives rise to a hole in the S wavefront and self-intersection of the T wavefront. Figure 6 shows corresponding wavefront sections (group-velocity surface) for slowness values in the neighbourhood of the conical point. Figure 6a shows the almost planar S-wavefront with a hole in the center. The S and T wavefronts are connected along the rim of the hole (for the purpose of representation a small gap is left between the two wavefronts). The slowness along the rim corresponds to the slowness at the conical point. The slower T wavefront is folded with self-intersections. This is shown in detail for two sections (b) $x \leq 0$ and (c) $y \geq 0$. Tips of so called swallowtail structures (see Rümpker and Thomson, 1994) of the T wavefront are marked in (b) and (c). At these tips the cusps due to the folding of the wavefront terminate. Note the two swallowtail tips along the symmetry plane ($x = 0$) in Figure 6b.

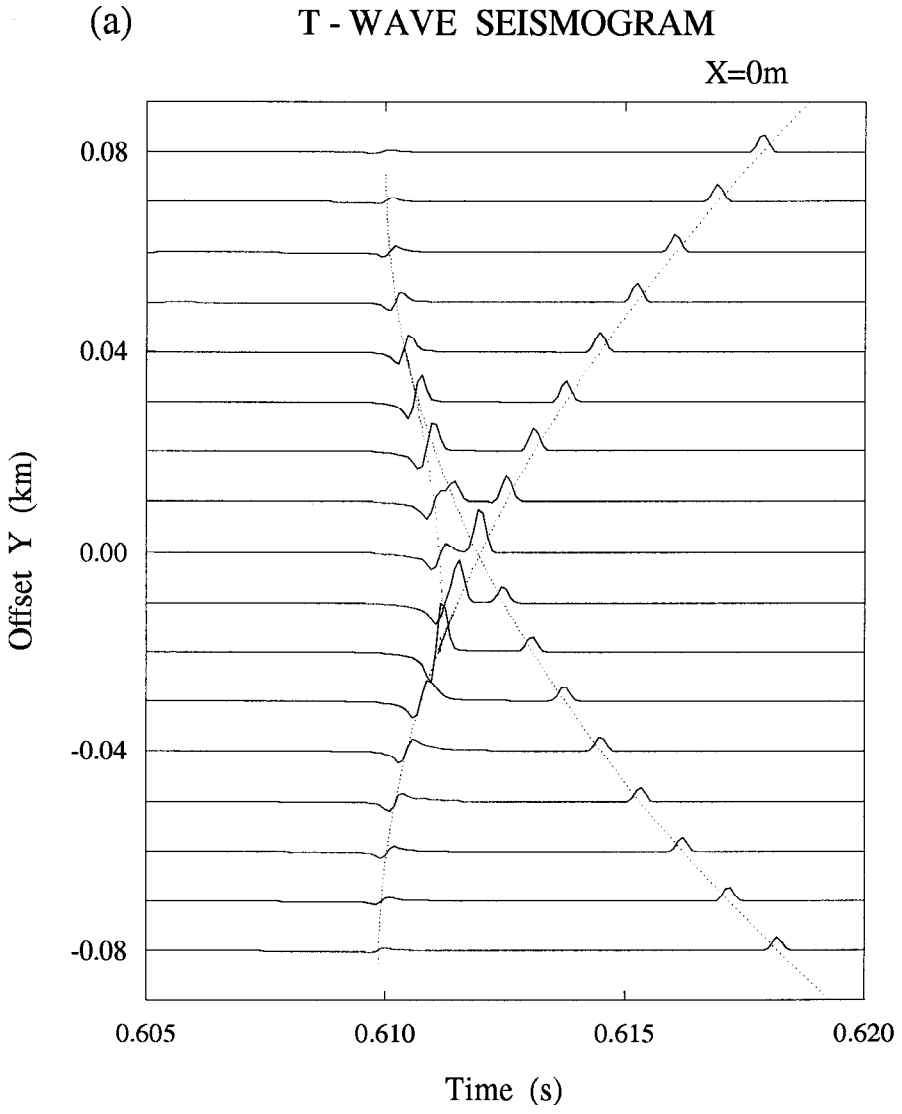

FIG. 7. T-wave seismograms for receiver positions along (**a**) $x = 0$ m and (**b**) $y = 0$ m with $z = 1000$ m. The source has components (1,1,0) and scalar waveforms are shown. The dotted line marks the traveltimes of geometrical arrivals.

Figure 7 shows corresponding T-wave seismograms for a point source with components (1,1,0) in the rotated coordinate system. Seismograms are calculated for receiver positions along lines (a) $x = 0$ and (b) $y = 0$ with $z = 1000$ km (corresponding to the wavefront sections shown in Figure 6). A pulse width of $\Delta t = 5 \times 10^{-4}$ s has been chosen to give a sufficient separation between individual arrivals. In (a) the T wavefront and the S wavefront are connected at approximately $y = \pm 80$ m and $t = 0.610$ s (S wave contributions are not shown here). At $y = 0$ there are two distinct geometrical arrivals: the first arrival results from the two out-of-plane saddle points of the T slowness surface in Figure 5. The superposed signals show characteristic Hilbert-transformed waveforms. The second is a superposition of two signals due to the maxima of the T slowness surface. On moving off the axis, the signals separate and merge with the saddle point arrivals to form a triplication of the T wave traveltime curve. Points where the three signals merge (near $y = -20$ m and $y = 30$ m) correspond to tips of swallowtail structures of the wave surface. This is related to Hilbert-transform-type waveforms with large amplitudes.

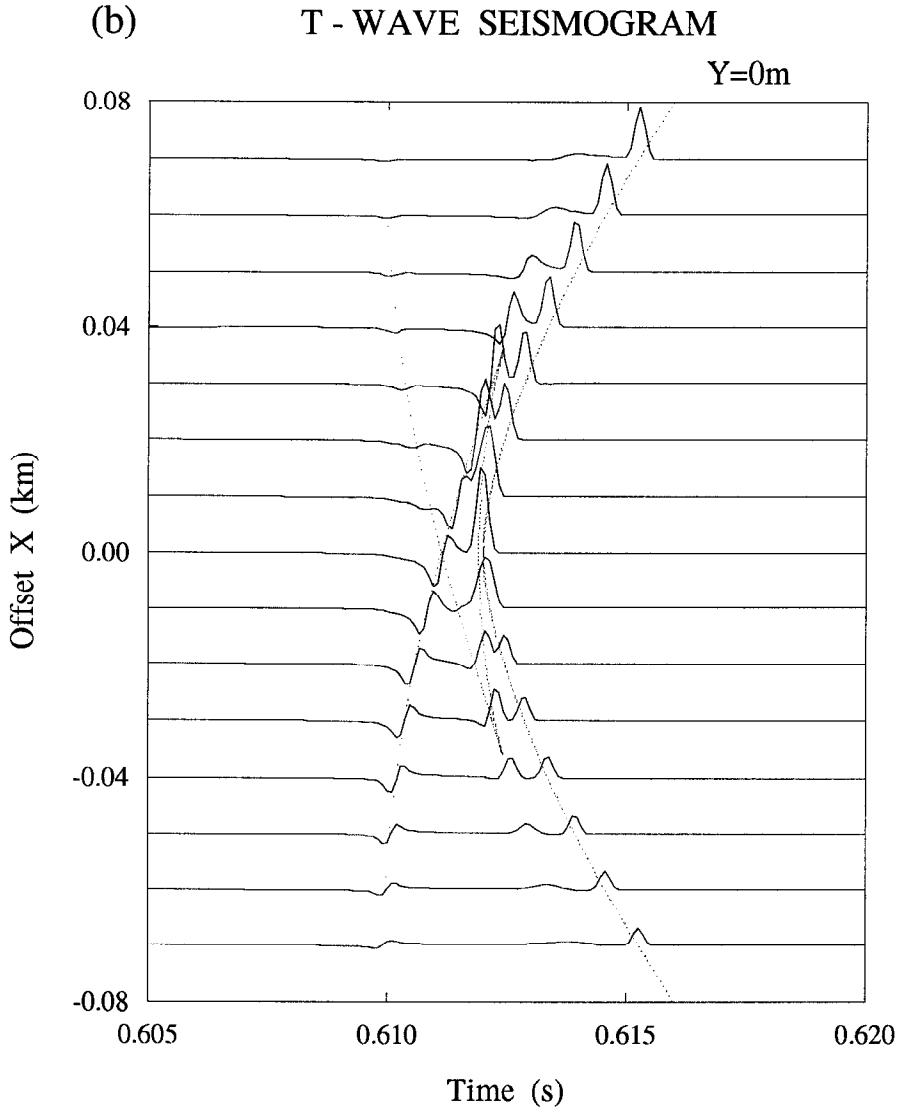

FIG. 7. (continued).

For a perpendicular line of receiver positions (Figure 7b) travel times are symmetrical with respect to the plane $x = 0$. However, there are strong variations in amplitude and net-waveforms. For $x > 0$, amplitudes of the first arrival are almost negligibly small compared to the first arrivals for $x < 0$, which clearly exhibit Hilbert-transformed waveforms. The amplitudes of merging signals near cusps at $y = \pm 30$ m are relatively large. However the net-waveforms differ dramatically as a results of different contributions form the signals merging here. Strong diffraction effects are shown off the cusps in particular for traces with offsets of ±40 m. Note that the traveltime curve shows three arrivals at $x = 0$. This agrees with findings in Figure 7a on taking into account that the intersection of the two wavefronts shown occurs not exactly at $y = 0$. In fact we have three arrivals at $y = 0$. However, the pulse width chosen does not allow the identification of all three arrivals on the seismogram trace.

NUMERICAL MODELLING RESULTS

To model the observations made in the physical experiments we assume a point source in a homogeneous medium with receiver positions that vary along circular arcs

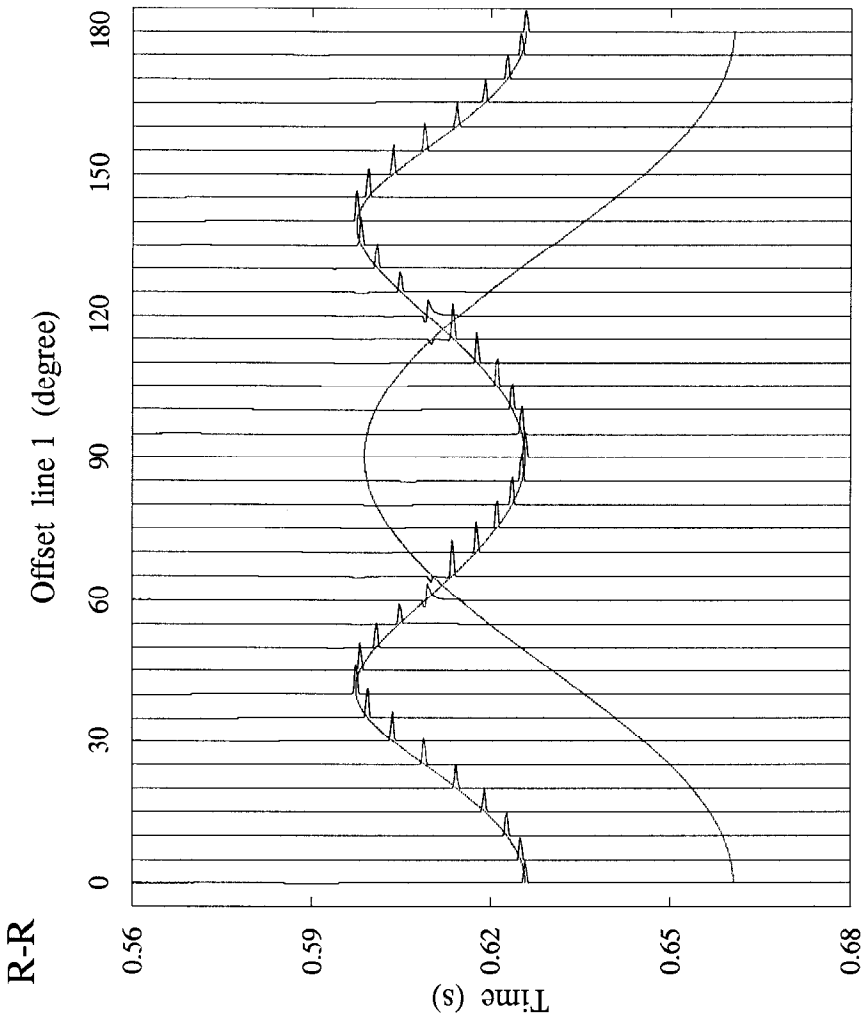

FIG. 8. S- and T-wave seismograms along Line 1 for (**a**) R-R polarization and (**b**) T-T polarization. An offset of 0° corresponds to the 3-axis, 90° to the 1-axis.

around the source. The source/receiver distance is taken to be equal to the diameter of the sphere. In doing so, we assume complete coupling between transmitter/receiver and surface of the sphere. We also neglect the effects of reflections from the spherical boundary, and of conversions. Seismograms are calculated for radial (in the sagittal plane) or transverse (perpendicular to this plane) source and receiver polarizations. Vertical (compressional) source/receiver components are not taken into account.

Line 1

We start with examples of numerically calculated seismograms along Line 1. In Figure 8 seismograms are shown for (a) radial (R-R) and (b) transverse (T-T) source and receiver combinations. The cross components, R-T and T-R, vanish since 3-1 is a symmetry plane. Seismogram traces have been calculated at intervals of 5°, slightly less than the 5.625° chosen in the physical experiment described. Traveltime curves for S and T waves are superposed and a pulse width of $\Delta t = 0.001$ s has been chosen. The maximum separation between the two shear wavefronts, near offsets of 30° and 150°, is approximately 0.42 s. For the transmitter/receiver combinations shown here, S- and T-wave arrivals appear on different traces. Note how the "gap" in the S wavefront near offsets 60° and 120° (due to the conical point) is "closed" by self-intersecting T wave arrivals.

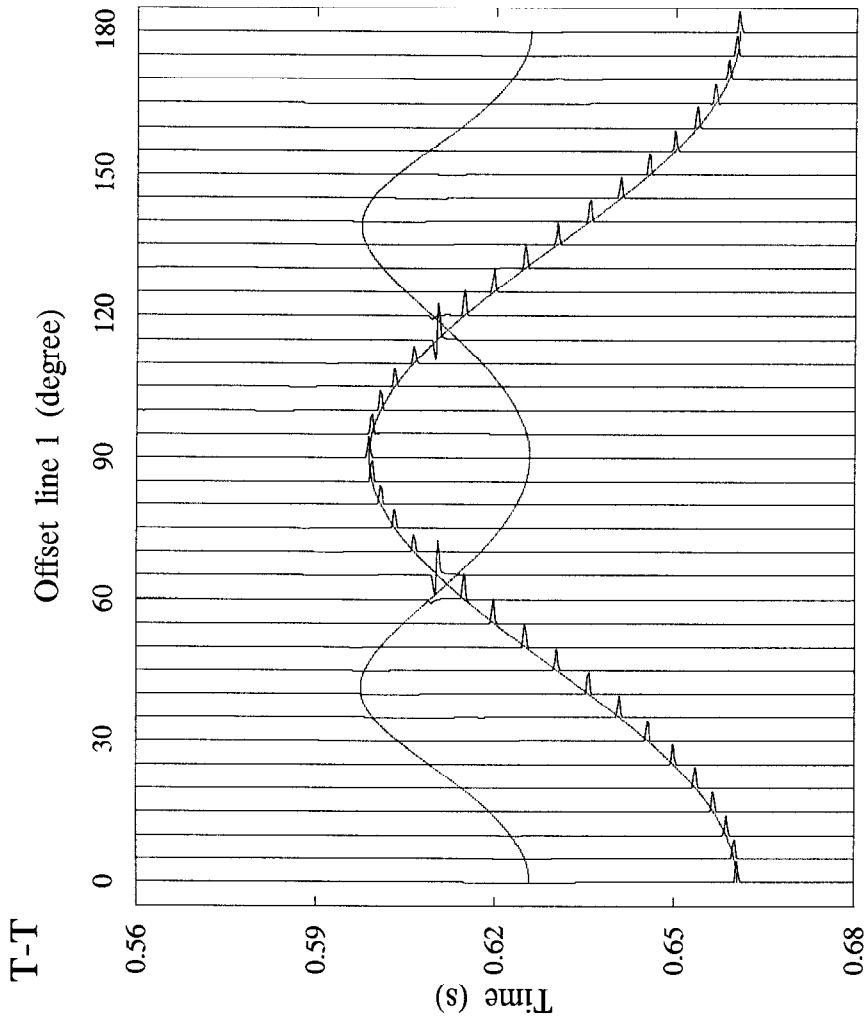

FIG. 8. (continued).

The R-R section (Figure 8a) shows S-wave arrivals only at offsets of 0° to 55° and 125° to 180°, and T-wave arrivals only in the interval from 60° to 120°. The waveforms in these intervals are simply smoothed δ-function pulses in correspondence with the assumed source waveform. Strong variations in waveform and amplitude are only found at offsets of 60° and 65° (and at 115° and 120°), where T-wave arrivals merge as a result of the swallowtail structure of the T wavefront. For the T-T section (Figure 8b) we have a similar but opposite situation with T-arrivals at offsets of 0° to 65° and 115° to 180°, and S-wave arrivals only from 70° to 110°. To analyze these waveforms in greater detail we calculated seismogram traces similar to those in Figure 7a but with the same transmitter/receiver configuration used here. The results are shown in Figure 9.

On the T-T section (Figure 9) two arrivals merge near a positive offset of $y = 40$ m. On comparison with Figure 7a we have to take into account that scalar waveforms are displayed there so as to show all geometrical arrivals in one set of seismograms. Note the reduction in relative amplitudes for the two arrivals at offset

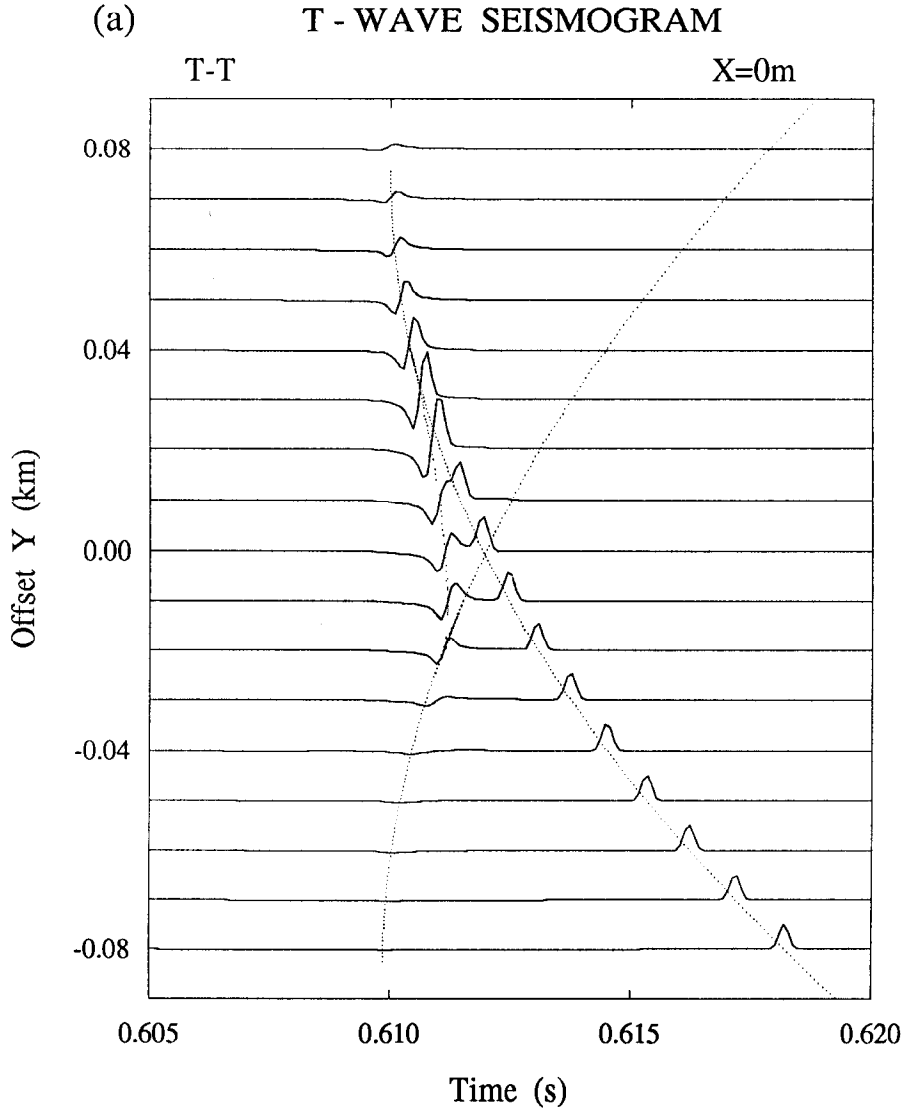

FIG. 9. T-wave seismogram for receiver positions along $x = 0$ m with $z = 1000$ m; source and receiver oriented in the T-direction

$y = 0$ in Figure 9 compared with Figure 7a. This is due to the elimination of two arrivals for this specific source/receiver configuration. The resulting seismogram traces can now be matched up with traces at offsets of 60° and 65° (or 115° and 120°) in Figure 8b. By comparing the T-T sections we find that offsets of 60° and 65° in Figure 8b correspond to offsets of –30 m and 20 m, respectively, in Figure 9. The Hilbert-transform-type waveform at 65°, therefore, indicates the merging of geometrical arrivals near a swallowtail tip on the T wavefront. Arrivals on the R-R sections (not shown) correspond to arrivals in Figure 8b in a similar manner.

The physical experiments did not show (at least it is not obvious) the waveform effects described here. A possible explanation for this could be the contamination of the seismograms with arrivals due to reflections from the spherical boundary, or to conversions. Another important effect is the pulse width or frequency used in the experiments. To illustrate this we calculated seismograms similar to those in Figure 8 but with a pulse width of 0.03 s. The results (Figure 10) show that individual signals, near offsets of 60° and 120°, cannot be separated for the pulse width chosen and that the waveform effects are less pronounced, though some waveform variability remains. Furthermore, in the physical modelling, rather than point sources and receivers, the transducers covered relatively large areas leading to spatial smearing of arrivals.

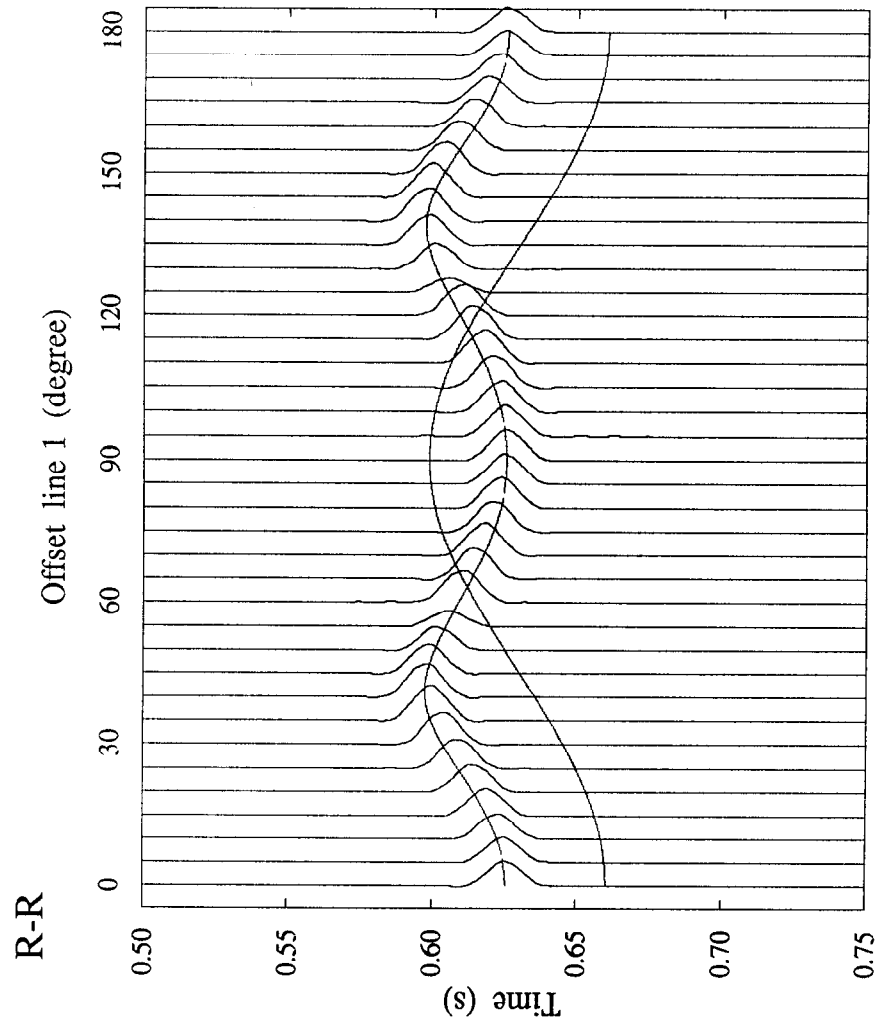

FIG. 10. Same as Figure 8, but for a pulse width of $\Delta t = 0.03$ s.

In the physical experiment, polarity reversals were shown on the cross-component sections, R-T and T-R, of Line 1 (a symmetry plane), whereas in our numerical analysis these cross-components vanish. To give a possible explanation for this we calculated displacement vectors corresponding to the first S- and T-wave arrivals for offsets along Line 1 with three different source orientations. The first two examples (Figure 11) with sources polarized radially (R) and transversely (T) correspond to the situation in the seismograms shown. The cross-components are zero in both cases. In a third example we assume a source orientation of 45° between R and T. In this case, the cross-components do not vanish and would indeed register with polarity reversals near offsets of 60° and 120° on a receiver polarized between R and T. The effect is strongest for 45° source and receiver orientations and gradually decreases for smaller or larger angles. This indicates that if the transducers were slightly misaligned or if they were not positioned exactly on the symmetry plane, there would be some energy on the cross-components and this could account for the physical modelling results.

Line 2

We now turn to examples of seismograms for source/receiver positions along Line 2 (Figure 12). Here, the zero offset corresponds to a position in the 3-1 symmetry

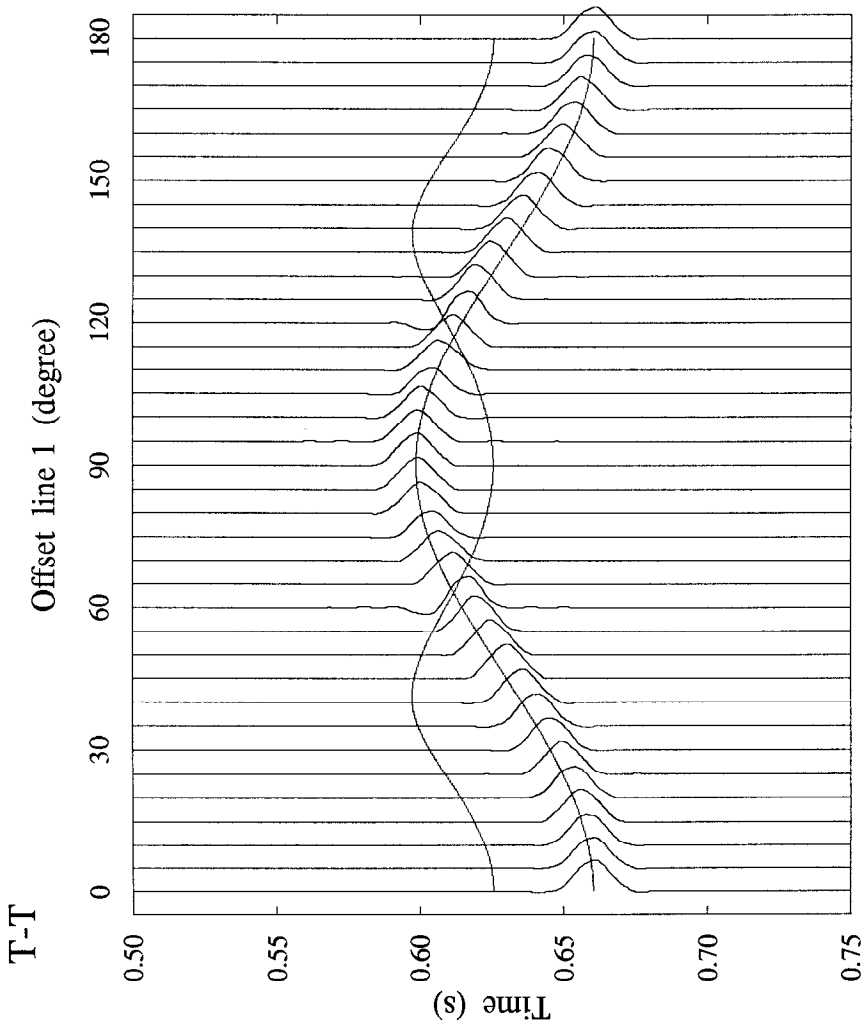

FIG. 10. (continued).

plane 45° off either axis. The cross-components (R-T and T-R) along Line 2 (Figure 12c) are generally nonzero. The separation between the two shear wavefronts ranges from 0.027 s near offsets of ±20° to 0.061 s at ±90° (along the 2-axis).

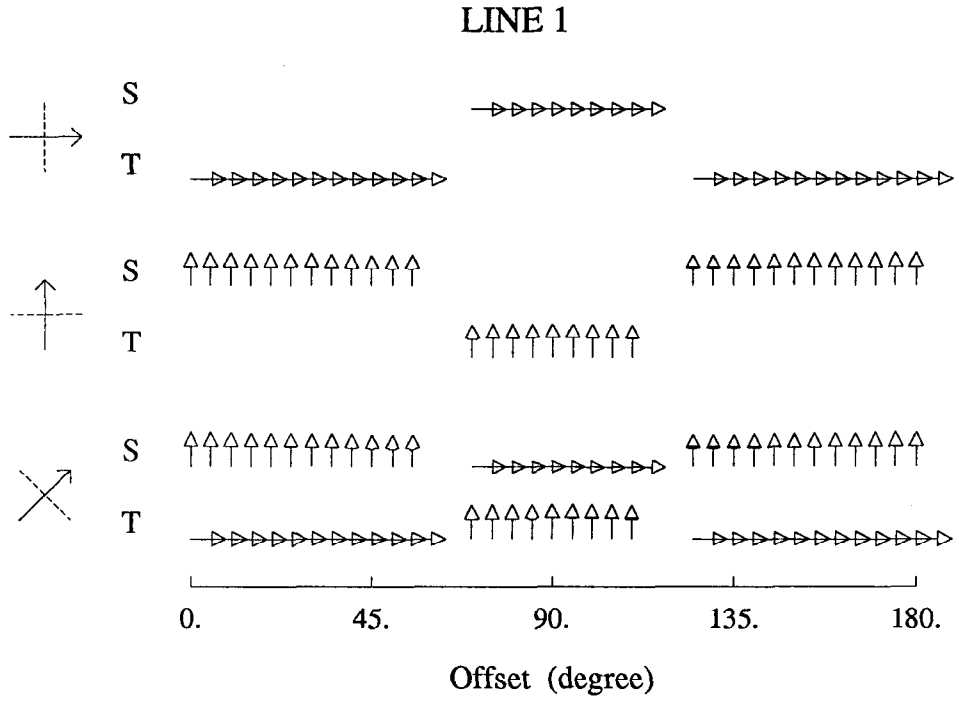

FIG. 11. The displacement corresponding to the profile along Line 1 for three source orientations as indicated by the arrows on the left. The dashed lines indicate the orientation of the cross-component.

On the R-R section (Figure 12a), the amplitude of the S-wave arrival vanishes in the symmetry plane and amplitudes are largest for offsets of about ±45°. The T-wave amplitudes are large in the symmetry plane with maximum amplitudes for offsets of about ±20°. There are no multiple arrivals and all waveforms are of δ-function type. On the T-T section (Figure 12b), the T-wave amplitude vanishes in the symmetry plane and remains relatively small for offsets up to ±15°. The amplitude reaches its maximum near ±35° and becomes only slightly smaller for larger offsets. The S-wave amplitude decreases gradually from its maximum in the symmetry plane to offsets of about ±45°, and then remains relatively constant.

On turning to the cross-component sections (Figure 12c), we note that results for the R-T and T-R combinations agree completely and therefore only one section is shown here. Physical results for these sections also seem to be quite similar, but there is a high noise level. The most striking feature here is the polarity reversal for both the S and T waves on passing across the symmetry plane, where the displacement vanishes. Note also that S and T have opposite polarization. This might give the impression of a Hilbert-transform-type waveform for lower frequencies. Amplitudes for S are largest at offsets of about ±40°, whereas the T wave amplitudes are largest at ±20°. For larger offsets, the amplitudes for both, S and T wave, decrease only slightly. We note that in the physical experiments seismogram traces show polarity reversal on the cross-components on passing the symmetry plane. However, due to the high noise level, travel times of the first shear wave arrivals are difficult to estimate from the observations.

To analyze the variation of the amplitudes along Line 2 in greater detail we calculated displacement vectors as function of offset for the two source orientations R and T. The displacement for a given source orientation depends on the polarization as a function of slowness. To find the polarization as a function of offset, the slowness of the Snell wave corresponding to a given receiver position has to be found. This can be done by finding the stationary point on the slowness surface for a given receiver position. For each receiver position along Line 2 there is only one stationary point on the slowness surface – there are no multiple arrivals. We have identified stationary points for receivers along Line 2. Traces of stationary points for receivers along Line 2 for S and T are shown in Figure 13 and the corresponding displacement vectors for two source orientations, R and T are shown in Figure 14. For a radial source orientation (Figure 14, top), the S-wave displacement is zero in the symmetry plane (zero offset), whereas the T-wave displacement reaches its maximum (in the R direction) here. For a transverse source (Figure 14, bottom), the S-wave displacement is largest (in the T-direction) in the symmetry plane, whereas the T-wave displacement vanishes. In both cases, the cross-component, indicated by the dashed line, for all wave types changes sign on passing the symmetry plane. Note that the total displacement changes only slightly.

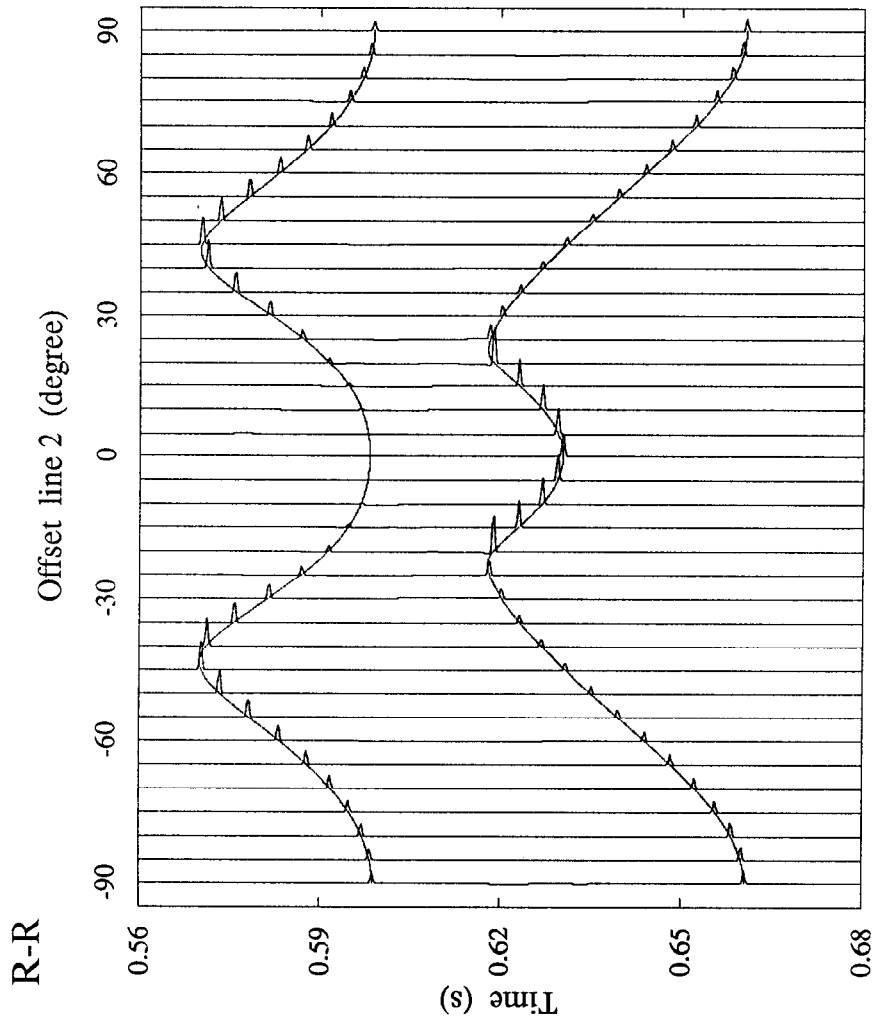

FIG. 12. S- and T-wave seismograms along Line 2 for (**a**) R-R, (**b**) T-T, (**c**) R-T and T-R polarizations. An offset of 0° corresponds to a position in the 3-1 plane half-way between the axes. Offsets of –90° and +90° correspond to shots along the 2-axis.

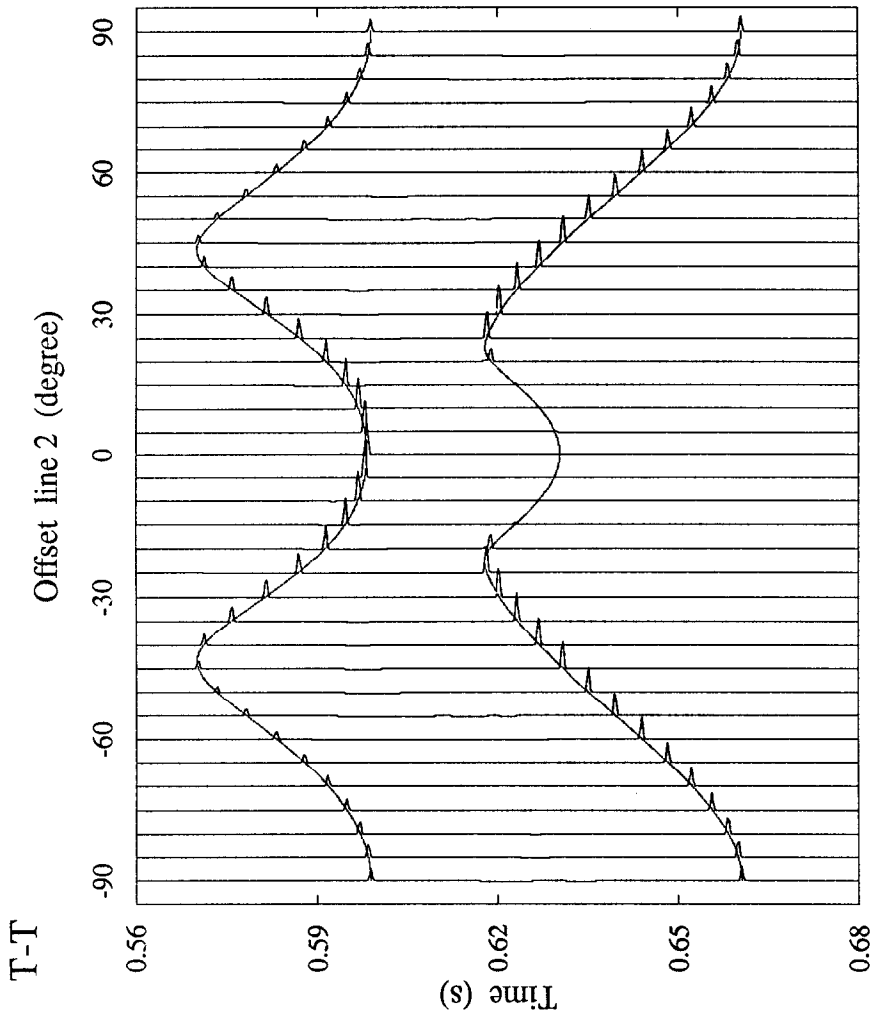

FIG. 12. (continued).

DISCUSSION

In this paper we have investigated effects of shear-wave propagation in orthorhombic Phenolic CE. In the first part of our study we showed examples of shear wavefronts and high-frequency seismograms calculated for receiver positions in the neighbourhood of an acoustic axis. Where the fast S wavefront exhibits a hole due to the conical point on the slowness surface, the T wavefront is folded with swallowtail structures. The corresponding seismograms show strong amplitude variations and Hilbert-transform-type waveforms due to the folding.

In the second part we calculated seismograms for two profiles through the PCE laminate to numerically model the physical experiment carried out by Brown et al. (1993). The first profile in this experiment (Line 1) corresponds to the 3-1 symmetry plane through the PCE sphere. The corresponding symmetry plane in slowness space exhibits a conical point. High-frequency seismogram traces calculated for transmitter/receiver positions close to the acoustic axis show multiple T-wave arrivals and Hilbert-transform type waveforms on the T-T and R-R components. The lateral

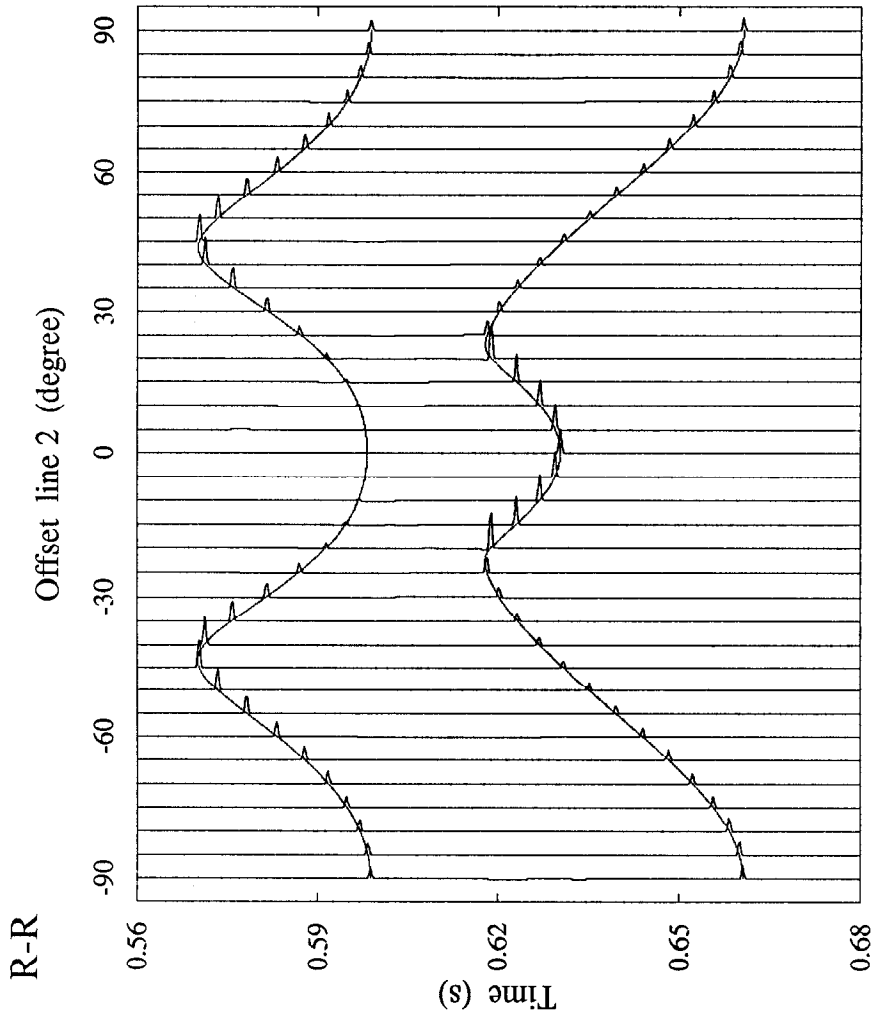

FIG. 12. (continued).

extent of the area on the sphere affected by these waveform effect is relatively small. In our examples, with an increment of 5° between offsets, only two neighbouring traces exhibit these waveform effects. However, effects are strongly diminished at lower frequencies and it remains doubtful whether they can still be detected with the present experimental setup. For this reason, a similar experiment is being shot on a larger phenolic sphere with over twice the radius.

Away from these, all traces contain only single arrivals of either S or T. The seismograms recorded by Brown et al. (1993) do show arrivals on the cross-components with a polarity reversal on passing the acoustic axis. This is not directly supported by our results where the cross-components vanish. However, a possible misalignment of transmitter and receiver with the symmetry axis, either in polarization or position, can cause sign changes on the cross-components for receiver positions crossing the acoustic axis. Another possibility seems to be a poorly defined symmetry plane due to inhomogeneities of the material.

Along Line 2, S- and T-wave arrivals are always completely separated. The cross-component profiles in our examples show polarity reversals for receivers crossing the symmetry plane The sign changes observed here cannot directly be

attributed to rapid variations of polarization in the neighbourhood of the acoustic axis. We consider the effects of small variations in the displacement together with the specific transmitter/receiver configurations to be a more likely explanation for this.

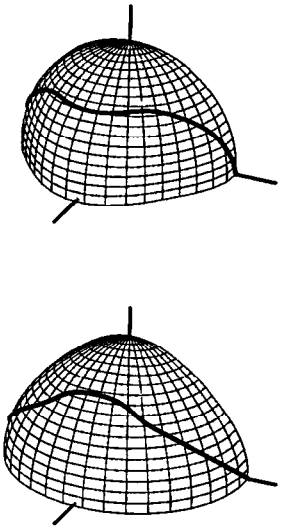

FIG. 13. Quadrants of the (top) S- and (bottom) T-wave slowness surfaces. The thick lines trace the positions of stationary points for receiver positions along Line 2.

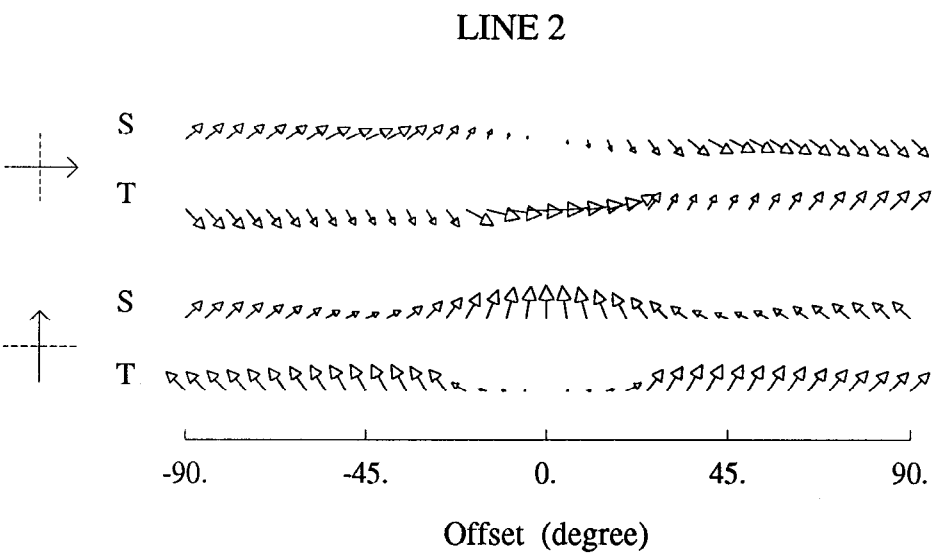

FIG. 14. The displacement corresponding to the profile along Line 2 for two source orientations as indicated by the arrows on the left. The dashed lines indicate the orientation of the cross-component. The displacement has been calculated from polarization vectors corresponding to slownesses along lines shown in Figure 13.

ACKNOWLEDGMENTS

GR is indebted to Colin Thomson for continuous and ongoing encouragement and support. Funding for GR is provided by a Queen's University Graduate Scholarships and by the German Academic Exchange Service (DAAD).

REFERENCES

Brown, R.J., Lawton, D.C., and Cheadle, S.P., 1991, Scaled physical modelling of anisotropic wave propagation: multioffset profiles over an orthorhombic medium: Geophys. J. Internat., **107**, 693-702.

Brown, R.J., Crampin, S., Gallant, E.V., and Vestrum, R. W., 1993, Modelling shear-wave singularities in an orthorhombic medium: Can. J. Expl. Geophys., **29**, 276-284.

Buchwald, V.T., 1959, Elastic waves in anisotropic media: Proc. R. Soc. A., **252**, 562-580.

Burridge, R., 1967, The singularity on the plane lids of the wave surface of elastic media with cubic symmetry: Quart. J. Mech. Appl. Math., **20**, 41-56.

Cheadle, S.P., Brown, R.J., and Lawton, D.C., 1991, Orthorhombic anisotropy: A physical seismic modeling study: Geophysics, **56**, 1603-1613.

Crampin, S., 1981, A review of wave motion in anisotropic and cracked elastic media: Wave Motion, **3**, 343-391.

Fedorov, F.I., 1968, Theory of elastic waves in crystals: Plenum Press.

Helbig, K., 1994, Foundations of anisotropy for exploration seismics: Pergamon Press.

Miller, G.F. and Musgrave, M.J.P., 1956, On the propagation of elastic waves in aeolotropic media. III. Media of cubic symmetry: Proc. Roy. Soc. Lond. A., **236**, 352-383.

Musgrave, M.J.P., 1970, Crystal acoustics, Holden-Day.

Musgrave, M.J.P., 1985, Acoustic axes in orthorhombic media: Proc. Roy. Soc. Lond. A., **401**, 131-143.

Rümpker, G. and Thomson, C.J., 1994, Seismic-waveform effects of conical points in gradually varying anisotropic media: Geophys. J. Internat., **118**, 759-780.